A micro-mechanical experimental study of highly/completely decomposed tuff granules

C.S. Sandeep[1] and M.C. Todisco[1], V. Nardelli[1], K. Senetakis[1*], M.R. Coop[2], S.D.N. Lourenco[3]

[1] City University of Hong Kong, Hong Kong SAR China
[2] University College London, UK
[3] University of Hong Kong
[*] (corresponding author), e-mail: ksenetak@cityu.edu.hk

ABSTRACT

In this paper, an experimental micromechanical study is presented investigating the contact mechanics and tribological behaviour of highly/completely decomposed tuff granules (denoted as H/CDT). The parent material was taken from two locations – named the top and bottom – from a recent landslide in Hong Kong and in this study the tested granules were obtainedfrom the parent material after drying and sieving processes. Basic material characterization was conducted quantifying the particle shape, the surface roughness and the strength of a set of grains. A set of twenty-nine monotonic inter-particle shearing tests were conducted on pairs of granules taken from the top and bottom of the landslide. It was found that the granules had very high friction angles at their contacts, in general greater in comparison to other materials reported in the literature. The slightly greater inter-particle friction for the granules taken from the top of the landslide might be because of their higher roughness in comparison to the ones from the bottom. Additional experiments were conducted to investigate the normal and tangential load-displacement response of the granules subjected to cyclic loading. A good curve fitting for the normal load-displacement response could be obtained by using very low apparent Young's moduli in the Hertzian model. In general, the decomposed tuff granules showed significant plastic response during the first normal load cycle, and this plastic behaviour continued for the subsequent third and fourth cycles. In the cyclic inter-particle shearing tests, the non-linearity and hysteresis increased for larger cyclic displacements, but the effect of the number of shearing cycles on the energy loss was generally small. Finally, a limited discussion is presented on the applicability of a theoretical model on the tangential load – displacement behaviour of the granules.

Keywords: Tangential stiffness; Inter-particle friction angle; Micro-mechanics; Completely decomposed tuff granules; Roughness;

1. Introduction

The development of the discrete element method (DEM) (after Cundall and Strack, 1979), has allowed the geotechnical research community to obtain insights into the complex behaviour of geological materials. Researchers have explored over the past decades different aspects of the behaviour of uncemented and cemented soils as well as problems related to the stability of geo-systems using DEM or coupled DEM/FEM models. One of the major problems in geotechnical engineering, which is quite complex, is the study of landslides and other natural granular flows; understanding of the mechanisms behind these soil/rock movements is challenging and it has attracted the attention by the scientific community in recent years including both numerical and large-scale or centrifuge model studies (e.g., Iverson, 1997, Calvetti and Nova, 2004, Van Asch et al., 2007, Hungr, 2008, Zhao and Shan, 2013, Turnbull et al., 2014, Alonso et al., 2015, Choi et al., 2015, 2016, Calvetti et al., 2017).

Using DEM for the study of landslide problems as well as other applications in geotechnical engineering, some important input parameters in the modelling are based on the grain contact behaviour, which include friction, normal and tangential load – deflection relationship and grain crushing. However, it was only recently achieved to build experimental apparatus which allowed the quantification of grain contact properties such as friction and stiffness, particularly in the study of sphere-sphere (or grain-grain) types of contacts (e.g., Cavarretta et al., 2010, 2011, Cole et al., 2010, Senetakis et al., 2013a, 2013b, Cole and Hopkins, 2016, Yang et al., 2016a, Sandeep and Senetakis, 2017, Nardelli et al., 2017). It is highlighted that even though significant new knowledge may be gained from numerical simulations of problems involving granular materials, experimental studies at the grain scale may also provide useful information as well as fundamental input parameters to be further utilized in DEM analyses. This may be particularly important if real soil grains are examined, which was one of the motivations of this study.

In their recent study, Sandeep et al. (2017) noticed relatively high friction angles at the contacts of decomposed (weathered) volcanic granules, which material is a type of coarse ash tuff and it was taken from the top of a recent landslide in Hong Kong. The high surface roughness of those granules as well as their soft nature might have contributed to this observed behaviour with reported inter-particle coefficient of friction (μ) ranging from about 0.30 to 0.60. Prior to this work, Senetakis et al. (2013b) reported μ values for Leighton Buzzard sand quartz grains, which material has much smoother surfaces, of the order of 0.17 as an average value. Based on many studies including the works by Cavarretta et al. (2011), Yang et al. (2016a), Cole and Hopkins (2016), Nardelli and Coop (2016) or Nardelli et al. (2017), it is acknowledged that the inter-particle friction may vary a lot depending on the nature and morphological characteristics of the grains in consideration. In general, brands of grains with more consistent surface characteristics may also have more consistent resultant inter-particle friction (for example, the quartz grains tested by Senetakis et al., 2013b). Materials with more inconsistent surface characteristics are also expected to demonstrate greater scatter in terms of inter-particle friction and other micromechanical parameters (e.g., Sandeep et al., 2017). Previous studies using the discrete element method have shown that the magnitude of the inter-particle friction at the contacts of the grains used as input may result in substantial different responses of granular materials (e.g., Sazzad and Suzuki, 2011, Huang et al., 2014). Wang and Yan (2012), studying the crushing behaviour of granular assemblies in DEM, acknowledged the important role of the inter-particle friction on the energy dissipation mechanisms. This means that it is important to quantify the inter-particle friction for different geological materials so that modelers can accordingly use different values (or ranges of values) in their analyses based on the problem in consideration.

In this study an attempt was made to enhance the database from the previous study by Sandeep et al. (2017), including additional experiments at the contacts of decomposed tuff granules taken from another location of the landslide. Differences with respect to the morphological characteristics of the granules from the different locations of the same landslide are acknowledged (including shape of granules and surface roughness) and additional experiments are conducted including grain crushing tests as well as cyclic normal and tangential load tests. It is noticed that these morphological and mechanical differences between granules from different locations may not represent precisely the in-situ conditions since the tested grains resulted from drying and sieving processes of the original material. However, this study may comprise an important first step to obtain useful micromechanical parameters of a material from a real landslide with the potential use as input in DEM simulations.

It worth noticing that for relatively smooth surfaces and of stiff contact behaviour, Sandeep and Senetakis (2018) reported a measurable initial plastic response during cyclic normal load tests on Leighton Buzzard sand quartz grains. This observation, which is in agreement with the previous study by Cavarretta et al. (2010) on reference grains, was attributed to asperity geometry and plastic response at the very early stage of the application of the normal load (with normal displacements of the order of 1 μm). However, the behaviour was fully elastic during the application of subsequent cycles (matching the elastic and non-linear behaviour of Hertzian type). So, in this study, apart from the investigation of the tribological behaviour of the decomposed tuff granules, additional experiments were conducted to understand the nature of their normal contact behaviour which is also important to be simulated in DEM analyses.

2. Materials, experimental methods and testing program

Equipment

Two major types of experimental apparatus were used in the study; one for the measurement of the normal and tangential contact behaviour and a second for the conduction of grain crushing tests. Several other techniques were also used for the characterisation of the materials tested.

The normal and tangential inter-particle loading tests presented in this paper were performed by means of a custom-made inter-particle loading apparatus at the City University of Hong Kong (after Senetakis and Coop, 2014, Nardelli, 2017). This apparatus is capable of conducting grain-scale experiments measuring the normal and tangential load – deflection behaviour at the contacts of sand-size grains from about 1 to 5 mm. The current version of the apparatus (Figure 1) mainly consists of a stiff loading frame (a) and a sled (b), which are both made of stainless steel, and three loading arms. Each of these arms is assembled connecting a linear stepper motor (c) and a load cell using stiff connections. The horizontal arms are connected to the sled, which is placed on a bearing system made up of three chrome steel balls. During each test, one of the two particles (d) is mounted on the sled and is enabled to move, while the other is rigidly connected to the vertical arm of the apparatus. The forces are measured using three high-resolution load cells (e) having a capacity of 100 N and a precision of 0.02 N. The displacement measurements are made using three non-contact eddy-current sensors (f), which are characterised by a very high-resolution (10^{-5} mm).

The whole apparatus is placed inside a Perspex chamber, which was built to enable the use of a humidity controller (Nardelli and Coop, 2016). This was installed in order to study the contact behaviour of particles under different environmental conditions, controlling the relative humidity within the range 15-85% and measuring the temperature inside the chamber. Two digital micro-cameras (g) are installed next to the apparatus to determine the precise contact location between the two particles tested and to take pictures during each test (Senetakis and Coop, 2014).

The single-particle crushing tests were carried out using a modified CBR apparatus, which was upgraded in order to study the crushing behaviour of particles (Wang and Coop, 2016; Todisco et al., 2017). The apparatus is constituted of a stiff loading frame and a loading machine and it is equipped with a load cell with a capacity of 1kN and an LVDT with resolution of 10^{-3} mm for the measurements of forces and displacements, respectively, along the axial direction of the device. Single-particle crushing tests were conducted in order to provide a basic characterisation of the possible range of compressive strength of the decomposed tuff granules and define the limits of the vertical confining force to be applied during the inter-particle shearing tests, avoiding premature particle breakage during testing.

Description of the landslide mechanism where the landslide material was obtained

Figure 2 shows the location of the landslide in the geological map of Hong Kong. Field observations reported that the landslide scarp was composed of highly to completely decomposed coarse ash tuff (H/CDT) of Jurassic/Cretaceous age (Irfan, 1999) overlain with a thin layer of residual soil (from 1.0 to 1.5m thick). The main scarp of the landslide source area was steeply inclined (<70°), while the slope of the above hillside covered by vegetation was about 15° and that of the hillside of the landslide about 20°-25°. The landslide source volume was approximately of 263m^3. The landslide was structurally-controlled as a relict joint plane with infills of iron and manganese oxides was visible on the failure surface. The landslide was probably triggered by the severe rainfall (409mm in 24h) that might have caused a perched water pressure to build up destabilizing further the slope. The landslide was classified as an open hillslope failure where the debris mass was not channelized, i.e. the debris mass does not flow into a stream course and therefore minimal water is added to the flow (Parry and Ng, 2010). According to GEO TGN34 (2012), this type of landslide can be provoked by initial sliding failure and the runout path can comprise intermittent sliding, rolling and bouncing of particles of different sizes.

Morphological description of the landslide material

The material was sampled at the top, middle and bottom of the landslide. For each location, soil was collected at the sides and middle of the runout path width in order to ensure spatial variability. This study refers to the top and bottom material taken in the middle of the runout path. Both dry and wet sieving were carried out in order to select the suitable size of the granules (based on limitations of the inter-particle loading apparatus and sample gluing technique). Based on this selection, possible differences of the morphological characteristics of the granules between the two locations could be obtained, even though it is emphasized that these differences, based on the sieved grains, are not necessarily representative of the evolution of the grain characteristics due to the land-sliding. Majorly, these differences can be only a reference for the subsequent study of particle crushing and inter-particle loading tests. Granules ranging from 1.18 to 2.36mm were selected after dry sieving and tested using the inter-particle loading and crushing apparatus in a quasi-dry state. This size range was selected with respect to the size limit of the inter-particle loading apparatus which is able to test particles ranging from about 1 to 5mm. Special attention was given to select the most regular in shape grains from the sieved material (in terms of normal and tangential – displacement tests) which is important to setup experiments in the apex-to-apex configuration as discussed by Senetakis and Coop (2014). The grading curves of the material referring to dry and wet sieving processes are illustrated in Figure 3.

Morphology assessment of the granules from the top and bottom of the landslide was carried out using the Krumbein and Sloss method (1963) which allows identifying the sphericity (S) and roundness (R) of a particle by visual comparison with shapes and outlines of reference projected sections of sand grains. Top and bottom granules (which were randomly collected for the shape quantifications) were characterised by similar sphericities with an average (S) value equal to 0.80, which indicates that they have a reasonably spherical shape. In terms of roundness, the top granules were in general less rounded (average R over fifteen grains = 0.55) than those from the bottom (average R over fifteen grains = 0.68). This can also be observed in representative SEM images of the granule surfaces (Figures 4a and c). The SEM images at higher magnification (Figures 4b and d) do not show notable differences in surface micro-topography between the top and bottom granules. The surface microstructure can be described for both top and bottom samples as dense without visible macro-pores and heterogeneous due to the presence of clay minerals, clay clusters, dispersed platy particles and a few silt grains that make the granule surfaces rough.

The roughness of the granules was quantified by means of white light interferometry. A small field of view of about 30x30μm was selected in order to minimise the percentage of undetected pixels within the images, which was quite significant for larger areas due to the low reflectivity of the material. As the percentage of the undetected pixels ranged between 5-7% even if smaller areas were used, a sputter coat of gold/palladium was applied on the granules to increase the material reflectivity. This technique allowed reducing the percentage of the undetected points on the particle surface to 1-2%. However as the coating, the thickness of which usually ranges between 2 and 20nm, might influence the surface roughness, its effect was investigated on quartz particles. The latter particles were considered as a reference material because fringes are usually easy to detect and undetected areas are less than 1% (Senetakis et al., 2013a, 2013b; Yang et al., 2016b). The roughness of fourteen coated H/CDT granules (seven from the top and seven from the bottom of the landslide) and three quartz particles was calculated as the RMS roughness, S_q (Equation (1)). This was achieved using a flattening function available in the software, which allows to separate the shape of the object from its surface topography.

$$S_q = \sqrt{\frac{1}{a \times b} \times \sum_{ij} Z_{ij}^2} \qquad (1)$$

In Equation (1), a and b are the number of points in the horizontal plane and Z is the deviation of each point from the mean height value. The average S_q of quartz particles (reference particles) before and after the coating process was equal to 329 and 295nm, respectively. The difference in S_q is relatively small and probably derives from the thin layer of coating that did not distribute uniformly on the surfaces with pronounced apexes and dimples. The layer may be thicker in the dimples and thinner at the apexes, resulting in less deviation of each point of the particle surface from the mean height value. Therefore, the S_q values of the coated H/CDT granules might be slightly underestimated. The average S_q of the coated granules from the top of the landslide was equal to 773nm with a standard deviation of ±131nm, while that of the bottom granules was equal to 572nm with a standard deviation of ±110nm. These roughness values are on average larger than those obtained for common natural sands, such as quartz or carbonate sand (S_q=510nm also over a field of view of 30x30μm-Nardelli and Coop, 2016). Figure 5 shows the flattened three-dimensional surface topography of a representative decomposed tuff granule from the bottom of the landslide. So, it is concluded that within this limited number of tests for particle morphology characterisation, the grains taken from the bottom of the landslide were relatively more rounded and of slightly smoother surface in comparison to the particles taken from the top of the landslide.

Testing programme and procedure

The testing programme consisted of twenty-nine monotonic inter-particle shearing tests, four cyclic normal loading tests, four cyclic tangential loading tests and sixty single-particle crushing tests. The cyclic normal loading tests were conducted to investigate possible effects of repeating the application of the normal load on the contact behaviour of the granules and the cyclic tangential tests were performed to quantify the energy loss during shearing under a cyclic mode.

Tables 1 to 3 indicate the granule size, the location in the landslide, the testing parameters and a summary of the test results. All the shearing tests (monotonic and cyclic) were conducted in a displacement-controlled mode at sliding rates that ranged from 0.03 to 0.20mm/h, while a constant rate of 0.30mm/h was adopted for the cyclic normal loading tests. A displacement rate of 0.1mm/min was used for the single-particle crushing tests. Prior to inter-particle shearing, a normal force of 0.5 or 1.0N was applied to the granules and maintained constant during the test. As the decomposed tuff granules were very weak (failure stress around 1MPa), a limited range of normal forces was used in order to avoid excessive particle damage during the inter-particle shearing tests.

The granules were glued on the brass mounts and left undisturbed for 24 hours before conducting the inter-particle shearing tests (Figure 1). The application of the vertical force was implemented in a way that an apex-to-apex configuration was obtained between the two particles prior to testing (Senetakis and Coop, 2014).

In the single-particle crushing tests, three descriptor diameters were measured by a Vernier calliper with a resolution of 0.01mm. In Table 1, d_{max} and d_{int} indicate the Feret diameters measured in the horizontal plane in the particle at-rest position, while d_{min} is the diameter measured in the vertical plane (i.e. the particle thickness). The failure characteristic stress was calculated as:

$$\sigma_f = \frac{P_f}{\pi \times \frac{d_{min}}{2} \times \frac{d_{int}}{2}} \qquad (2)$$

In Equation (2), P_f is the maximum force recorded from the test. Equation (2) assumes a tensile failure (more sophisticated crushing mechanisms are beyond the purpose of this work) and adopts the geometric mean of the d_{min} and d_{int} as the failure area. This allows some consideration of the effect of the particle morphology, especially in the case of elongated particles, as shown in Todisco et al. (2017).

3. Results and discussion

Single-particle crushing tests

The single-particle crushing test results were expressed in terms of the probability of surviving of grain splitting (Weibull, 1951) against the failure characteristic stress. All the tests showed a brittle type of behaviour with a sudden drop of the load after reaching a peak value. Figure 6 presents the survival probability of granules from the top and bottom of the landslide. The characteristic stress at a survival probability of 37% is around 1MPa for both locations. The two curves tend to overlap up to a survival probability of 40% and below this value, the granules from the bottom of the landslide, which were slightly more rounded, appear stronger in comparison to the granules from the top. Wang and Coop (2016) and

Todisco et al. (2017) found that sphericity and local roundness (calculated from the asperities at the contact) could influence the particle strength. It is noted that the highly/completely decomposed (H/CDT) granules are very weak if compared to the strength of other sand particles of similar size as reported in the literature (Nakata et al., 1999, 2001, Todisco et al., 2017). For example, characteristic stresses at 37% survival probability of 11 and 45MPa were found for similar size limestone (shown in the figure) and quartz sand grains, respectively (Todisco et al., 2017).

Normal load-displacement cyclic tests

For two (out of four) experiments where the normal load-displacement response of the granules was investigated, the plots are provided in Figures 7 and 8 for H/CDT granules from the top and bottom of the landslide, respectively. Both tests showed a highly non-linear response (i.e. non-linear increase of the normal load against the displacement). The response was found to be highly plastic with a substantial increase of the modulus at the contact from the first to the second loading (similar observations were recorded for the other two pairs of grains). For simplicity, the modulus computation, which in reality corresponds to an apparent value, was derived based on Hertzian fitting (Hertz, 1882), based on Equation (3):

$$P = \frac{4 \times \left(R^*\right)^{\frac{1}{2}} \times E^* \times \delta^{\frac{3}{2}}}{3} \quad (3)$$

where R^* is the equivalent particle radius computed from Equation (4), P is the normal load, δ is the normal displacement and E^* is the equivalent Young's modulus (the latter being the fitting parameter of the model to the experimental curve).

$$\frac{1}{R^*} = \frac{1}{R_1} + \frac{1}{R_2} \quad (4)$$

In Equation (4), R_1 and R_2 corresponded to the average radius of the three dimensions of the two particles in contact, measured using a Vernier calliper. The average radius of pairs of granules from both top and bottom of the landslide was equal to about 1 mm. The equivalent Young's modulus E* is correlated with the apparent Young's modulus (E_1 and E_2) through Equation (5):

$$\frac{1}{E^*} = \frac{1-\nu_1^2}{E_1} + \frac{1-\nu_2^2}{E_2} \tag{5}$$

where, it is assumed that $E_1 = E_2$, for the Poisson ratio $\nu_1 = \nu_2$ which was taken equal to 0.3 as reported by Irfan (1983) for decomposed volcanic rocks in Hong Kong. Although the Hertzian curves could fit reasonably well the experimental ones, it is highlighted that the values of Young's moduli are only apparent, as the normal-loading response of this material exhibits plasticity. Currently a direct comparison with the real (mineral) Young's modulus would be difficult to make due to the complex mineralogy of this material.

During the first normal loading cycle, the apparent Young's modulus was found equal to 180 and 160 MPa for the material from top (Figure 7) and bottom (Figure 8) of the landslide, respectively. After reloading, the grains were found to have much higher values of Young's modulus, i.e., 1700 and 1400 MPa for the top and bottom material shown in Figures 7 and 8, respectively. This means that the apparent stiffness at the contacts of the H/CDT granules had an increase of one order in magnitude from the first to the second loading and that these moduli were found markedly smaller in magnitude in comparison to the corresponding normal load-displacement tests conducted on other types of grains reported in the literature. For example, testing Eglin grains, which are mainly constituted of silica, Nardelli et al. (2017) reported values of apparent E between 52 to 94GPa, whilst a value of 11GPa was obtained for a biogenic carbonate sand (Nardelli and Coop, 2016).

Figure 9 gives a summary of the total set of four cyclic normal loading tests showing the effect of the number of loading cycle on the apparent Young's modulus for the decomposed tuff granules. It is noticed that even though the major change of Young's modulus took place from the first to the second cycle, some increase is still observed for the third and fourth cycles for all the tested samples (for example from about 1.4 to 1.5 GPa and from about 1.7 to 1.8 GPa). In their recent study, Sandeep and Senetakis (2018) showed that for Leighton Buzzard sand quartz grains, there was only a slight increase of Young's modulus from the first to the second cycle (from about 70 to 73 GPa), but thereafter, no further change was observed for subsequent cycles. So that for the quartz grains tested by Sandeep and Senetakis (2018), which consist of very smooth surfaces, the normal contact response was majorly elastic with traces of some plastic deformation during the first cycle. But for the very soft and rough tuff granules of this study, plastic deformations are predominant during the first cycle and they continue to be observable in subsequent cycles of normal loading.

Inter-particle friction and tangential stiffness during monotonic shearing tests

Typical horizontal (or shearing) force-displacement curves of granules from the bottom and top of the landslide are presented in Figure 10, where no significant difference can be observed between the materials from the two locations. On average, large displacements were needed before reaching constant values of horizontal forces, i.e. the steady-state condition. This might be justified by the large contact diameter, i.e. 0.33 and 0.26mm at 1 and 0.5N normal load, respectively, calculated theoretically by the Hertz model for elastic sphere-sphere contact (Hertz, 1882). By applying the Hertz theory, a Young's modulus of the material equal to 0.16GPa was found through curve fitting of the tests (as a representative value). For comparison, a pair of quartz grains with an apparent Young's modulus of 50GPa, the size of the H/CDT particles (2mm) and with a Poisson's ratio of 0.1 will have a contact diameter of 0.05mm at 1N normal load and a steady-state condition is reached at around 0.02-0.03mm (Sandeep and Senetakis, 2017).

In Figure 11, the mobilised inter-particle coefficient of friction (μ_{mob}) is plotted against the horizontal displacements for representative tests from both the top and bottom H/CDT granules. Beyond a horizontal displacement of about 80 to 100μm, the mobilised friction reached a steady-state, denoted as μ. For some of the tests, some slight oscillation of the horizontal force was observed, even though relatively large displacements were reached. In general, it was not observed a very clear effect of the applied normal load on the resultant μ_{mob} or μ. The μ values of the bottom material are slightly larger than the top ones, with average values over all the tests of 0.44 (bottom grains) and 0.37 (top grains), respectively. Also, the μ values of the bottom granules were less scattered than the top ones, with values that ranged from 0.35 to 0.54 with a standard deviation of ±0.05. A larger range was found for the top granules, with values of μ between 0.22 to 0.56 with a standard deviation of ±0.09. The differences in the observed μ values between top and bottom granules might be related to the greater roughness values observed for the material taken from top of landslide.

The inter-particle friction angles were found greater for the H/CDT granules, with average values between 20^{o} to 24^{o}, in comparison to the data in the literature for quartz sand grains tested by Senetakis et al., (2013a, 2013b) and Sandeep and Senetakis (2018), who found friction angle values between about 7^{o} to 17^{o}. But the quartz grain surfaces were much smoother and harder than the material tested in this study. On the other hand, the friction angles for the H/CDT granules are much closer to the values obtained for a biogenic carbonate and Eglin sand reported in Nardelli and Coop (2016) and Nardelli et al. (2017), the roughnesses of which (around 500-600nm) were similar to that of H/CDT grains. The values of the inter-particle friction measured for H/CDT are also larger than those determined by Nardelli et al. (2016) for two natural scaly clays, which were characterised by a scaly mesostructure and smooth tectonised surfaces. This probably means that both shape and surface roughness have an effect on the test results for clay materials. In the case of H/CDT, roughness values of 500-700nm might be compared to the size of clay platelets that lie on the surface in a disaggregated way as shown in the SEM images (Figure 4). At such low normal loads, larger tangential forces might be needed to overcome rough asperities which could not be plastically deformed or abruptly removed. The large contact diameters of the landslide material due to their very low values of apparent Young's modulus might also contributed to the high inter-particle friction values.

Figures 12 gives representative results for the tangential stiffness (K_T) plotted against the displacement. These results correspond to a nominal vertical normal load of 1N. The tangential stiffness was computed differentiating the horizontal (tangential) force over the horizontal displacement similar to Senetakis et al. (2013b). The tangential stiffness of both bottom and top granules showed similar trends and values, ranging from about 25 to 80 N/mm at a horizontal displacement of 10^{-4}mm. These were very low compared to the data available in the literature (e.g. Senetakis et al., 2013a, Sandeep and Senetakis, 2018, Nardelli and Coop, 2016). The rapid reduction of K_T with increasing sliding displacement reflects the highly non-linear response at the contacts of the decomposed tuff granules.

Application of the Mindlin and Deresiewicz model to the experimental results

Figure 13 gives a comparison between the tangential force-displacement curve obtained through the present experiments (showing a representative test) and the widely used Mindlin and Deresiewicz model (after Mindlin and Deresiewicz, 1953). According to that theory, the horizontal force-displacement curve follows a non-linear elastic behaviour initially and purely plastic behavior afterwards. Based on the Mindlin and Deresiewicz model, the value of the initial tangential stiffness ((K_{t0}) was obtained using Equation (6):

$$K_{t0} = 8 \times \alpha \times \left(\frac{2-\nu_1}{G_1} + \frac{2-\nu_2}{G_2}\right)^{-1} \tag{6}$$

where α is the Hertzian contact area, G_1 and G_2 are the shear modulus of the two grains in contact (taken as 85 MPa based on that the apparent Young's modulus was computed for the given pair as 220MPa). Even though the theoretical curve seems to fit better the initial part of the experimental one, there is a poor agreement between two curves in the later stages. For Eglin sand, Nardelli et al. (2017) observed the similar variations between experimental and Mindlin and Deresiewicz curves which they ascribed to roughness (which affects the contact area calculation), hardness and complex particle geometry.

Cyclic inter-particle shearing tests

Figure 14 presents the results of four cyclic shearing tests conducted on the bottom granules varying the amplitude of displacement as 0.005, 0.01, 0.02 and 0.04mm. For each test, four loading-unloading cycles were performed under a displacement rate of 0.06mm/h. Note that with increasing the displacement amplitude, higher non-linearity in the horizontal force – displacement relationship was observed with a substantial increase of the loop area, which implies an increase of energy dissipation (i.e. damping) at the contacts of the granules. The energy dissipation (D) was expressed with the following classical formula used in systems dynamics:

$$D(\%) = \frac{1}{4\times\pi} \times \frac{\Delta W}{W} \times 100 \quad (7)$$

where W is the elastic energy stored into the system and ΔW is the energy loss (ΔW is equal to the area of the closed loop). D of the second cycle was found equal to about 8%, 22%, 24% and 28% for displacement amplitude of 0.005, 0.01, 0.02 and 0.04mm, respectively. In general, the effect of the number of cycles on the energy dissipation of a given pair of H/CDT granules was found relatively small. Based on the test results shown in Figure 14, the secant stiffness (K_s) was computed which is defined as the slope connecting the end points of the closed loop. The K_s values based on the second cycle of the cyclic tests is plotted in Figure 12 along with the monotonic tangential stiffness. It is shown that at a displacement of about 0.005mm, the K_s value is much greater than the corresponding range of tangent values, however these differences become smaller at greater displacements.

4. Conclusions

The contact behaviour of highly/completely decomposed tuff granules (H/CDT) taken from a recent landslide in Hong Kong was investigated in terms of monotonic and cyclic force-displacement response, inter-particle coefficient of friction and stiffness. The material characterisation showed that the H/CDT granules from the top and bottom of the landslide had similar sphericity, strength at failure (characteristic stress at 37% survival probability equal to around 1MPa) and surface roughness (500-700nm). The top granules were slightly less rounded than those from the bottom but this difference was too small to infer any link between morphology and particle strength. The inter-particle normal and tangential force-displacement behaviour did not show any significant difference between top and bottom granules. They were characterised by an average coefficient of friction of 0.44 and 0.37 for bottom and top granules, respectively, which is relatively large compared to other geo-materials. Perhaps, the rough surfaces of the H/CDT granules as well as their low apparent Young's modulus might have contributed to these high μ values. The slightly greater friction values for the top granules could be related with their greater roughness in comparison to the bottom granules.

It was noticed that beyond a large horizontal displacement of about 80 to 100μm, the mobilised coefficient of friction reached a steady-state. The soft nature of the granules might have contributed to this behaviour, as larger contact areas were expected during normal loading, thus larger displacements are required to reach a steady-state during shearing. Cyclic normal contact tests for a limited set of granules indicated that the response was highly plastic and hysteretic during the first cycle which resulted in a sensible increase of the normal contact stiffness during the second cycle. A slight increase was also observed after the application of a third and fourth cycle in the normal direction, even though this increase was more moderate in comparison to the observations during the second cycle. By applying the Hertz model, the apparent Young's modulus of the granules was found to be within a narrow range of about 0.16 to 0.22 GPa during the first loading cycle and between about 1.40 and 1.70 GPa during the second cycle, respectively. These values were significantly lower in comparison to reported data in the literature for other soils. Cyclic shearing tests indicated values of the contact damping to range from about 8% to 28% for displacement amplitudes from 0.005 to 0.04mm. The model proposed by Mindlin and Deresiewicz was applied to the experimental horizontal force – displacement curve and for a representative test this comparison was shown in the study. It was revealed that even though the model matched better the experimental data at the initial part of the curve, in general the highly non-linear response of the granules at their contacts resulted in notable differences between theoretical and measured curves at greater displacements.

ACKNOWLEDGEMENTS

The study was fully supported by a grant from the Research Grants Council of the Hong Kong Special Administrative Region, China (Theme-based research project Scheme "Understanding Debris Flow Mechanisms and Mitigating Risks for a Sustainable Hong Kong" - Project No. Project No. T22-603/15 N (CityU 8779012)). The Geotechnical Engineering Office (GEO) of the Civil Engineering and Development Department of Hong Kong is acknowledged for their help during the collection of the landslide material.

REFERENCES

Alonso E., Zervos A., Pinyol N.M. (2015). Thermo-poro-mechanical analysis of landslides: from creeping behaviour to catastrophic failure. Géotechnique, 63(3), pp. 202-219.

Calvetti F., Nova R. (2004). Micromechanical approach to slope stability analysis, In: Darve, F., Vardoulakis, I. (Eds.), Degradation and Instabilities in Geomaterials, CISM Courses and Lectures no. 461 Springer, Wien, pp. 235-254.

Calvetti F., di Prisco C.G., Vairaktaris E. (2017). DEM assessment of impact forces of dry granular masses on rigid barriers. Acta Geotechnica, 12(1), pp. 129-144.

Cavarretta, I., Coop, M.R., O' Sullivan, C. (2010) The influence of particle characteristics on the behavior of coarse grained soils. Geotechnique, 60(6), pp. 413-423.

Cavarretta I., Rocchi I., Coop M.R. (2011). A new interparticle friction apparatus for granular materials. Canadian Geotechnical Journal, 48(12), pp. 1829–1840.

Choi, C.E., Au-Yeung, S.C.H., and Ng, C.W.W. (2015). Flume investigation of landslide granular debris and water runup mechanisms. Géotechnique Letters, 5(1), pp. 28-32.

Choi, C.E., Goodwin, G., Ng, C.W.W., Chu, H.K., Kwan, J.S.H., and Pun, W.K. (2016). Coarse granular flow interaction with slit-structures. Géotechnique Letters, 6(4), pp. 1-8

Cole D.M., Hopkins M.A. (2016). The contact properties of naturally occurring geologic materials: experimental observations. Granular Matter, 18, pp. 61-77.

Cole D.M., Mathisen L.U., Hopkins M.A., Knapp B.R. (2010). Normal and sliding contact experiments on gneiss. Granular Matter, 12, pp. 69–86.

Cundall P.A., Strack O.D.L. (1979). A discrete numerical model for granular assemblies. Géotechnique, 29, pp. 49–65.

Geotechnical Engineering Office, Civil Engineering and Development Department, The Government of the Hong Kong Special Administrative Region, (2012). Guidelines on Assessment of Debris Mobility for Open Hillslope Failures, GEO Technical Guidance Note No. 34 (TGN 34).

Hertz H. (1882). Uber die Beruhrang fester elastischer Korper (On the contact of elastic solids). Journal der rennin und angewandeten Mathematik. 92, pp. 156–171.

Huang, X., Hanley, K.J., O'Sullivan, C., Kwok, C.Y. (2014). Exploring the influence of interparticle friction on critical state behaviour using DEM. International Journal for Numerical and Analytical Methods in Geomechanics, 38(12), 1276-1297.

Hungr O. (2008). Simplified models of spreading flow of dry granular material. Canadian Geotechnical Journal, 45, pp. 1156–1168.

Irfan T.Y. (1983). Foundation design of caissons on volcanic rocks: a technical review, GCO Report No. 13/83

Irfan T.Y. (1999). Characterization of weathered volcanic rocks in Hong Kong. Quarterly Journal of Engineering Geology, 32, pp. 317-348.

Iverson R.M. (1997). The physics of debris flows. Reviews of geophysics, 35(3), pp. 245-296.

Krumbein W.C., Sloss L.L. (1963). Stratigraphy and Sedimentation. W. H. Freeman and Company, San Francisco.

Mindlin R. D., Deresiewicz H. (1953). Elastic spheres in contact under varying oblique forces. Journal of Applied Mechanics, 20, pp. 327-344.

Nakata Y., Hyde A.F.L., Hyodo M., Murata H. A probabilistic approach to sand particle crushing in the triaxial test. Geotechnique, 49(5), 567-583.

Nakata Y., Kato Y., Hyodo M., Hyde A.F.L., Murata H. One-dimensional compression behaviour of uniformly graded sand related to single particle crushing strength. Soils and Foundations, 41(2), 39-51

Nardelli V., Coop M.R., Vitone C., Chen S. (2016). The inter-scale behaviour of two natural scaly clays. Géotechnique Letters, 6 (3), pp. 205-210.

Nardelli, V., An experimental investigation of the micromechanical contact behavior of soils, in: Architechture and Civil Engineering Department, City University of Hong Kong, 2017.

Nardelli V., Coop M.R., Andrade J.E., Paccagnella F. (2017). An experimental investigation of the micromechanics of Eglin sand. Powder Technology, 312, pp. 166-174.

Nardelli V., Coop M.R., (2016). The micromechanical behaviour of a biogenic carbonate sand, In: Proc. of VI Italian conference of researchers in geotechnical engineering CNRIG– Geotechnical Engineering in Multidisciplinary Research: from Microscale to Regional Scale, 22-23 Sept., Bologna, Italy, Procedia Engineering, 158, pp. 39-44.

Parry S., Ng K.C. (2010). The assessment of landslide risk from natural slopes in Hong Kong: an engineering geological perspective. Quarterly Journal of Engineering Geology and Hydrogeology, 43, pp. 307-320.

Sandeep C.S., Senetakis K. (2017). Exploring the micromechanical sliding behavior of typical quartz grains and completely decomposed volcanic granules subjected to repeating shearing. Energies, 10, 370.

Sandeep, C.S., Senetakis, K. (2018). Grain-scale mechanics of quartz sand under normal and tangential loading. Tribology International, 117, pp. 261-271.

Sandeep, C.S., Todisco, M.C., Senetakis, K. (2017) Tangential contact behaviour of weathered volcanic landslide material from Hong Kong. Soils and Foundations, 57, pp. 1097-1103.

Sazzad, Md. M., and Suzuki, K. (2011). Effect of Interparticle Friction on the Cyclic Behavior of Granular Materials Using 2D DEM. J. Geotech. Geoenviron. Eng., 137(5), pp. 545–549.

Senetakis K., Coop M.R. (2014). The development of a new micro-mechanical inter-particle loading apparatus. Geotechnical Testing Journal, 37(6), pp. 1028-1039.

Senetakis K., Coop M., Todisco M.C. (2013a). Tangential load-deflection behaviour at the contacts of soil particles. Géotechnique Letters, 3(2), pp. 59-66.

Senetakis K., Coop M., Todisco M.C. (2013b). The inter-particle coefficient of friction at the contacts of Leighton Buzzard sand quartz minerals. Soils and Foundations, 53(5), pp. 746-755.

Todisco M.C., Wang W., Coop M.R., Senetakis K. (2017). Multiple contact compression tests on sand particles. Soils and Foundations, 57, pp. 126-140.

Turnbull B., Bowman E.T., McElwaine J.N. (2014). Debris flows: Experiments and modelling. C.R. Physique, http://dx.doi.org/10.1016/j.crhy.2014.11.006

Van Asch T., Malet J.-P., Van Beek L., Amitrano D. (2007). Techniques, advances, problems and issues in numerical modelling of landslide hazard, Bulletin de la Société Géologique de France, 178(2), pp. 65-88.

Wang J. and Yan H.B., (2012). DEM Analysis of Energy Dissipation in Crushable Soils, Soils and Foundations, 52(4), 644–657.

Wang W., Coop M.R. (2016). An investigation of breakage behaviour of single sand particles using a high-speed microscope camera. Géotechnique, 66(12), pp. 984-998.

Weibull W. (1951). A statistical distribution function of wide applicability. J. Appl. Mech., pp. 293–297.

Yang, L., Wang, D., Guo, Y., Liu, S. (2016a). Tribological behaviors of quartz sand particles for hydraulic fracturing. Tribology International, 102, 485–96.

Yang H, Baudet B.A.,Yao T. (2016b). Characterization of the surface roughness of sand particles using an advanced fractal approach. Proceedings of the Royal Society A: Mathematical, Physical and Engineering Sciences. 10.1098/rspa.2016.0524.

Zhao J., Shan T. (2013). Coupled CFD-DEM simulation of fluid-particle interaction in geomechanics, Powder Technology, 239, pp. 248-258.

TABLE 1 Single-particle crushing tests

Material location in landslide	Number of tests	d_{max} [mm]	d_{int} [mm]	d_{min}[mm]	Characteristic stress at 37% survival probability [MPa]
TOP	30	2.28	2.23	1.84	0.78
BOTTOM	30	2.74	2.25	1.90	1.17

TABLE 2 Monotonic inter-particle sliding tests

Material location in landslide	Test code	Rate [mm/h]	Vertical force, F_v [N]	Inter-particle coefficient of friction, μ	Total horizontal path, $\delta_{h,tot}$ [mm]
TOP	T2-1-0.2	0.2	1	0.56	0.16
	T3-1-0.2	0.2	1	0.33	0.20
	T4-1-0.2	0.2	1	0.38	0.15
	T5-1-0.2	0.2	1	0.37	0.18
	T1-1-0.06	0.06	1	0.44	0.15
	T2-1-0.06	0.06	1	0.47	0.14
	T3-1-0.06	0.06	1	0.27	0.12
	T1-1-0.03	0.03	1	0.37	0.12
	T1-1-0.04	0.04	1	0.41	0.15
	T1-0.5-0.2	0.2	0.5	0.46	0.28
	T2-0.5-0.2	0.2	0.5	0.36	0.22
	T3-0.5-0.2	0.2	0.5	0.22	0.19
	T4-0.5-0.2	0.2	0.5	0.32	0.20
	T5-0.5-0.2	0.2	0.5	0.28	0.19

(Continued)

BOTTOM	B1-1-0.2	0.2	1	0.45	0.15
	B2-1-0.2	0.2	1	0.50	0.19
	B3-1-0.2	0.2	1	0.47	0.15
	B1-1-0.06	0.06	1	0.42	0.18
	B2-1-0.06	0.06	1	0.40	0.10
	B3-1-0.06	0.06	1	0.54	0.12
	B1-1-0.03	0.03	1	0.42	0.05
	B2-1-0.03	0.03	1	0.47	0.08
	B3-1-0.03	0.03	1	0.43	0.06
	B1-0.5-0.2	0.2	0.5	0.43	0.17
	B2-0.5-0.2	0.2	0.5	0.43	0.16
	B3-0.5-0.2	0.2	0.5	0.51	0.15
	B1-0.5-0.06	0.06	0.5	0.35	0.12
	B2-0.5-0.06	0.06	0.5	0.37	0.14
	B3-0.5-0.06	0.06	0.5	0.45	0.15

TABLE 3 Cyclic inter-particle sliding tests

Material location in landslide	Type of cycling	Number of cycles	Rate [mm/h]	Vertical force, Fv [N]	Amplitude of horizontal displacement (mm)
Top	Normal	4	0.3	1	-
Top	Normal	4	0.3	1	-
Bottom	Normal	4	0.3	1	-
Bottom	Normal	4	0.3	1	-
Bottom	Tangential	4	0.06	1	0.005
Bottom	Tangential	4	0.06	1	0.01
Bottom	Tangential	4	0.06	1	0.02
Bottom	Tangential	4	0.06	1	0.04

FIGURES

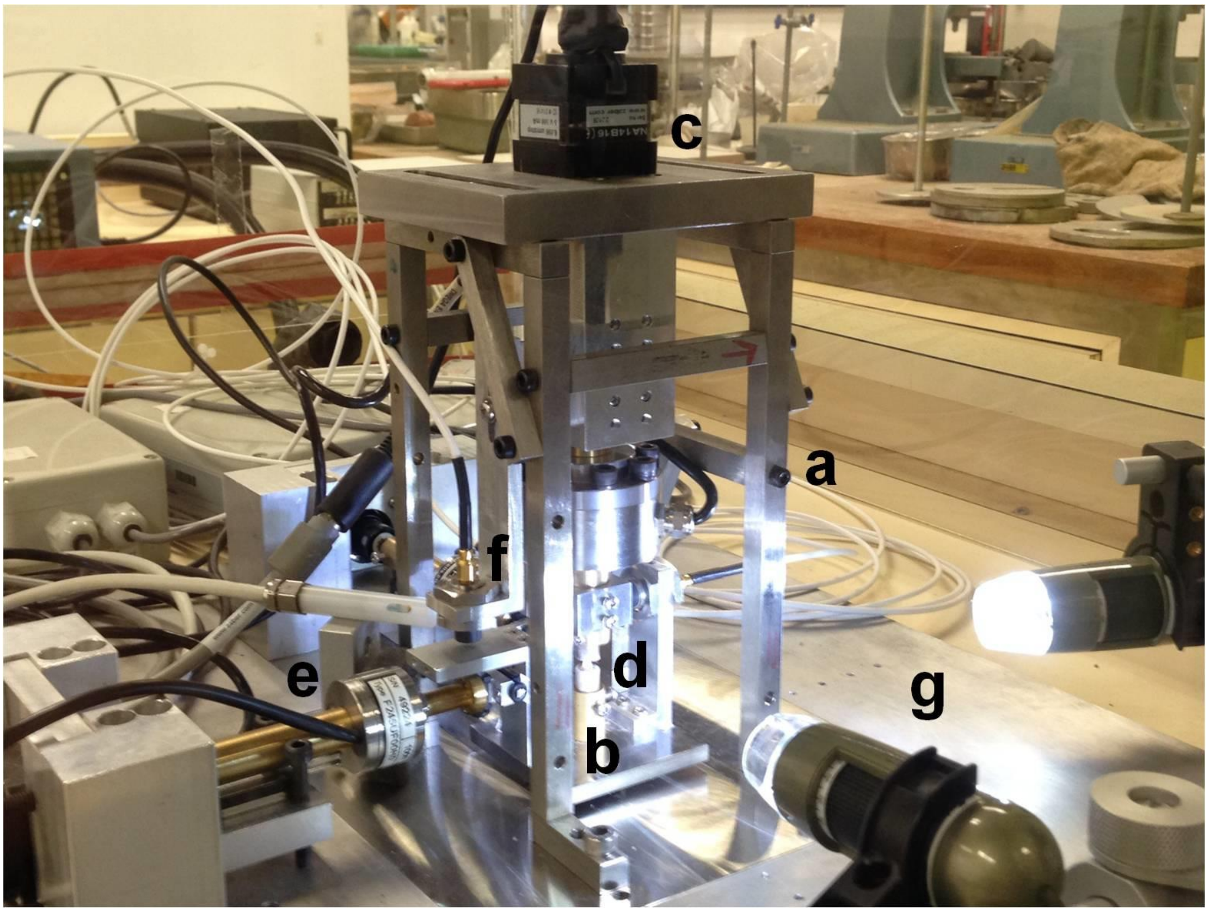

Figure 1 Inter-particle loading apparatus: a) loading frame; b) sled; c) stepper-motor; d) sand particles; e) load cell; f) eddy-current sensor; g) digital micro-cameras.

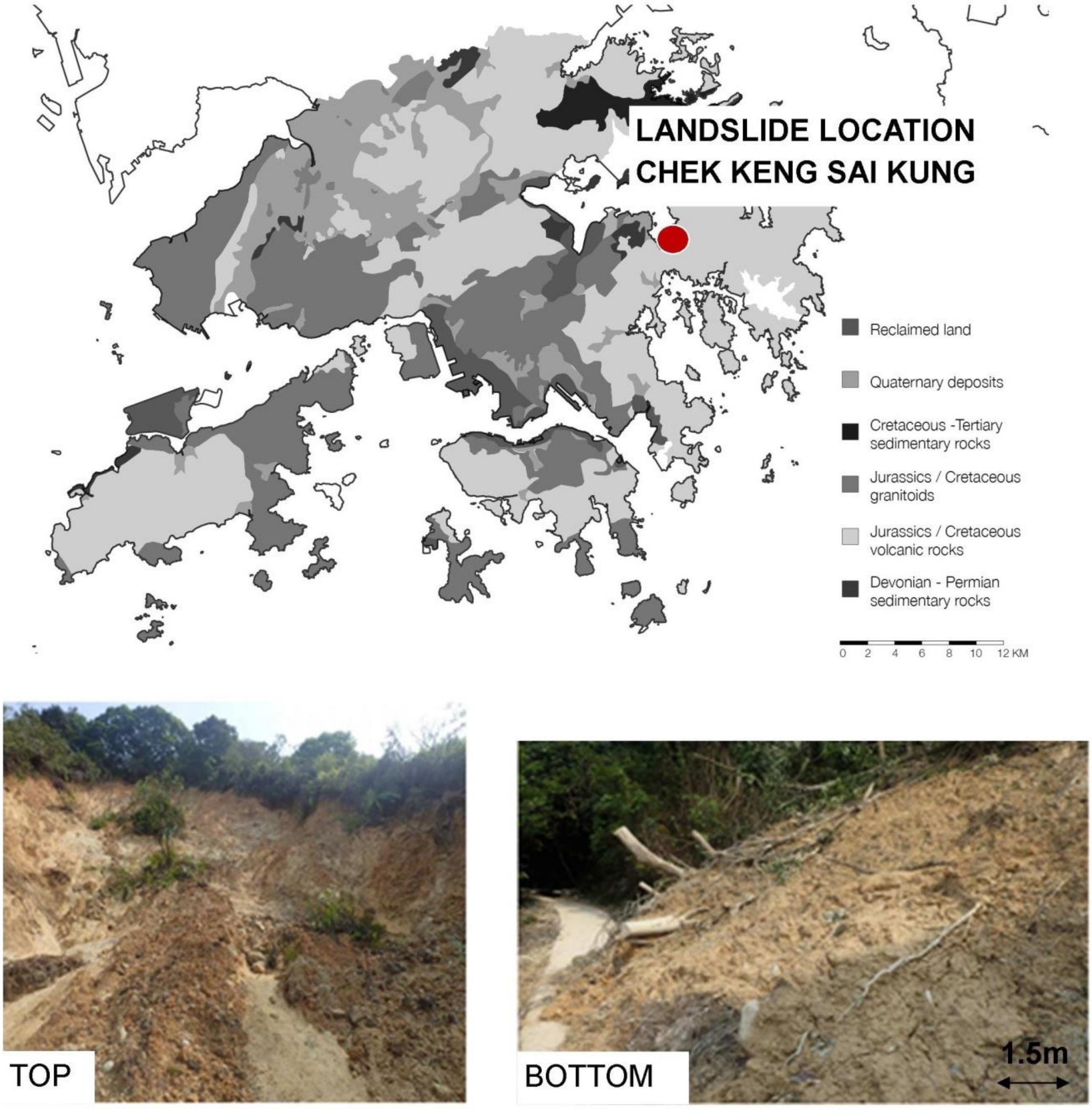

Figure 2 Location of the landslide (where the tested material was taken) in the geological map of Hong Kong and photographs of the top and bottom of the landslide taken in September 2016.

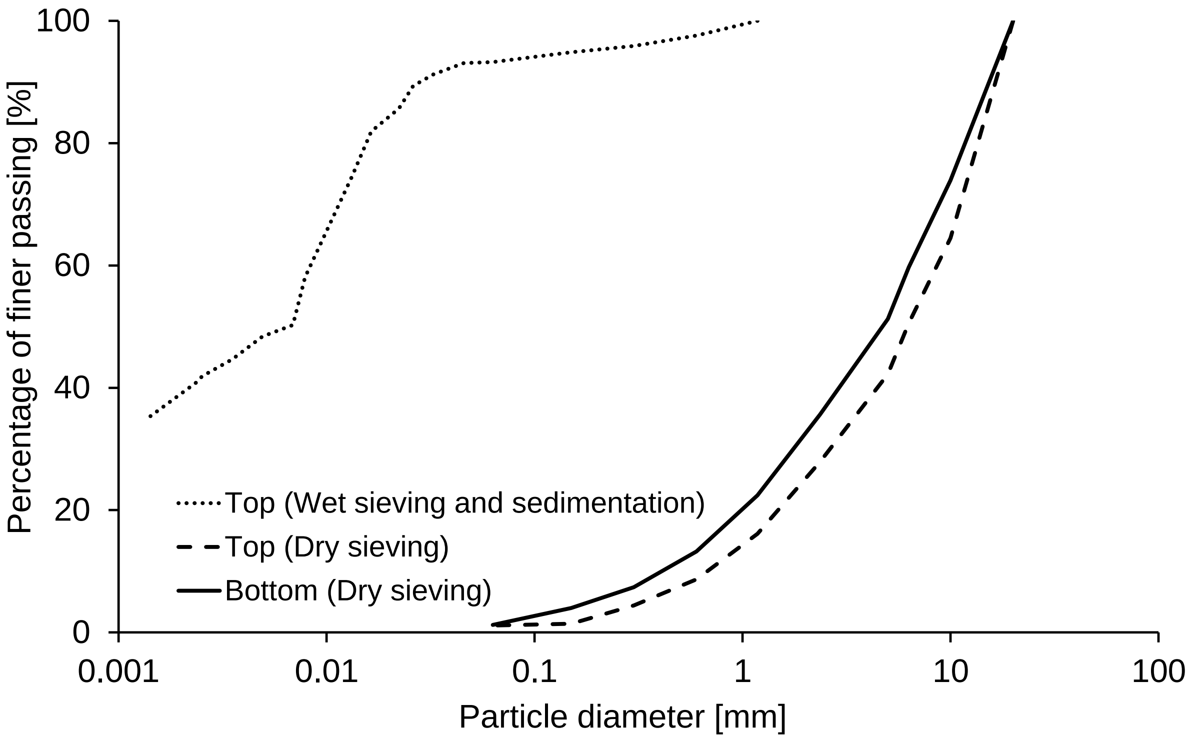

Figure 3 Particle size distribution of the decomposed tuff granules from the top and bottom of the landslide.

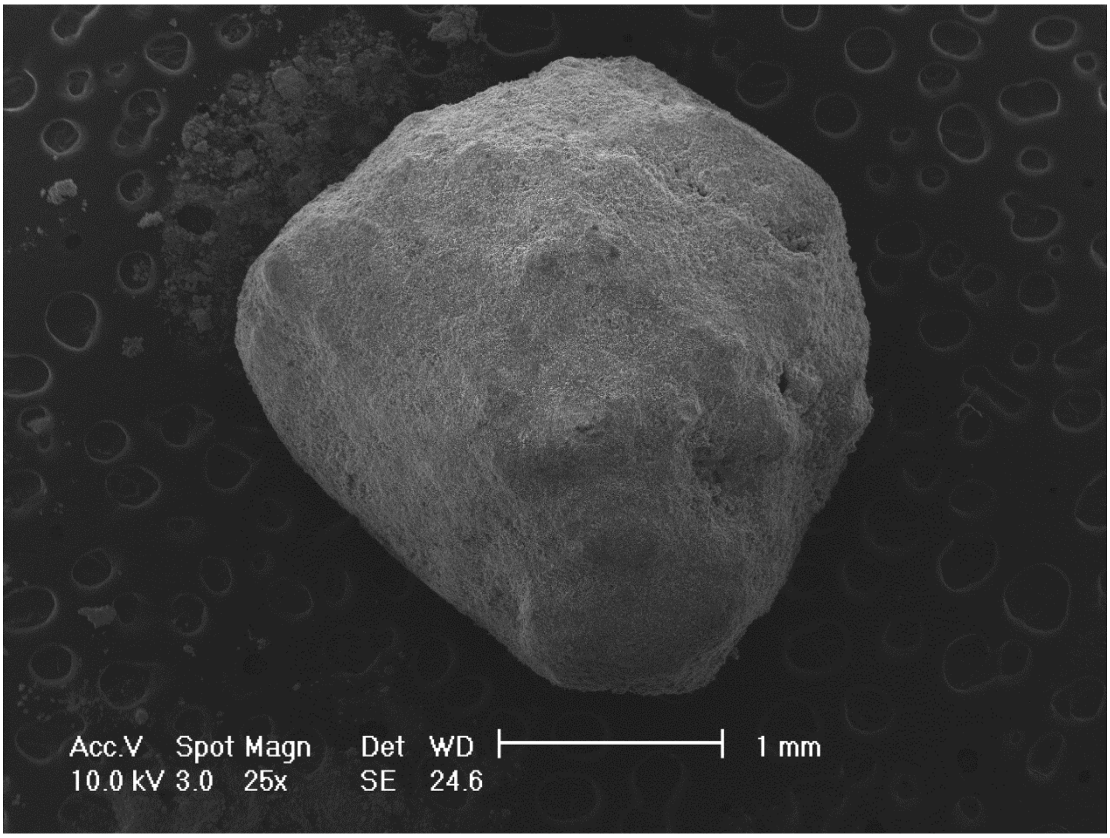
Acc.V Spot Magn Det WD 1 mm
10.0 kV 3.0 25x SE 24.6

a)

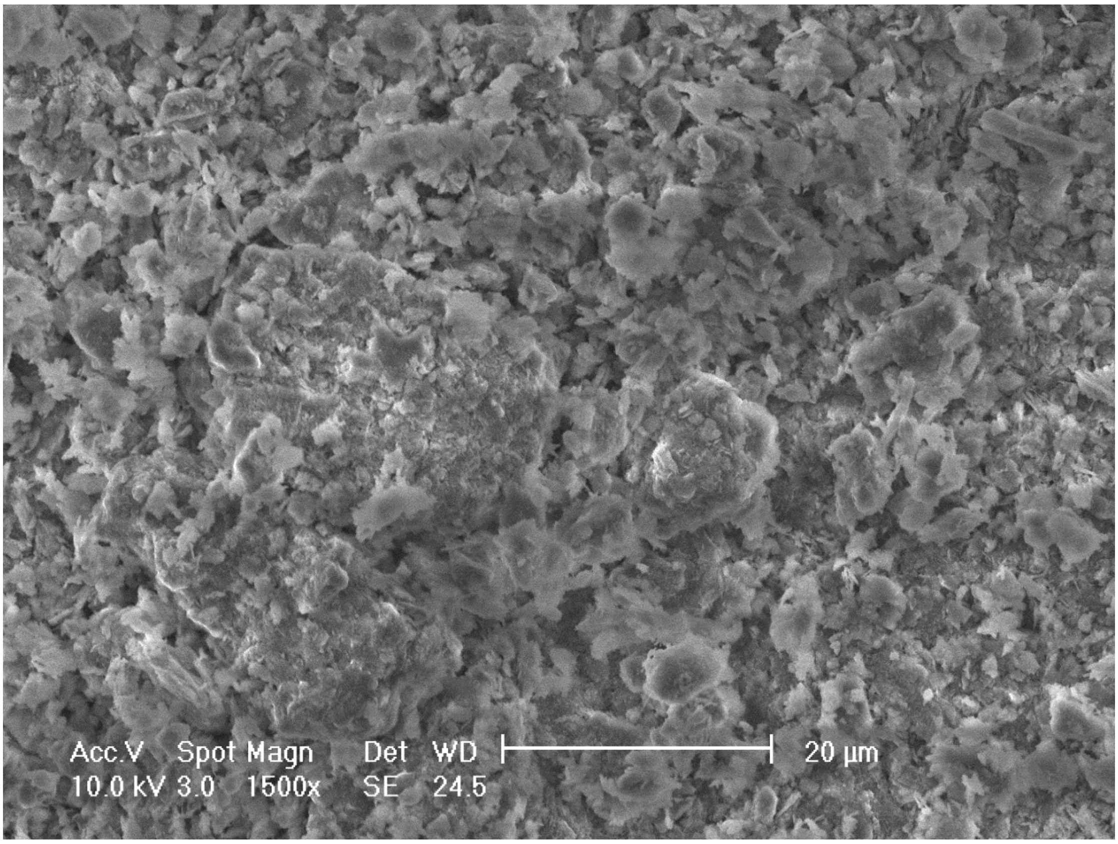
Acc.V Spot Magn Det WD 20 µm
10.0 kV 3.0 1500x SE 24.5

b)

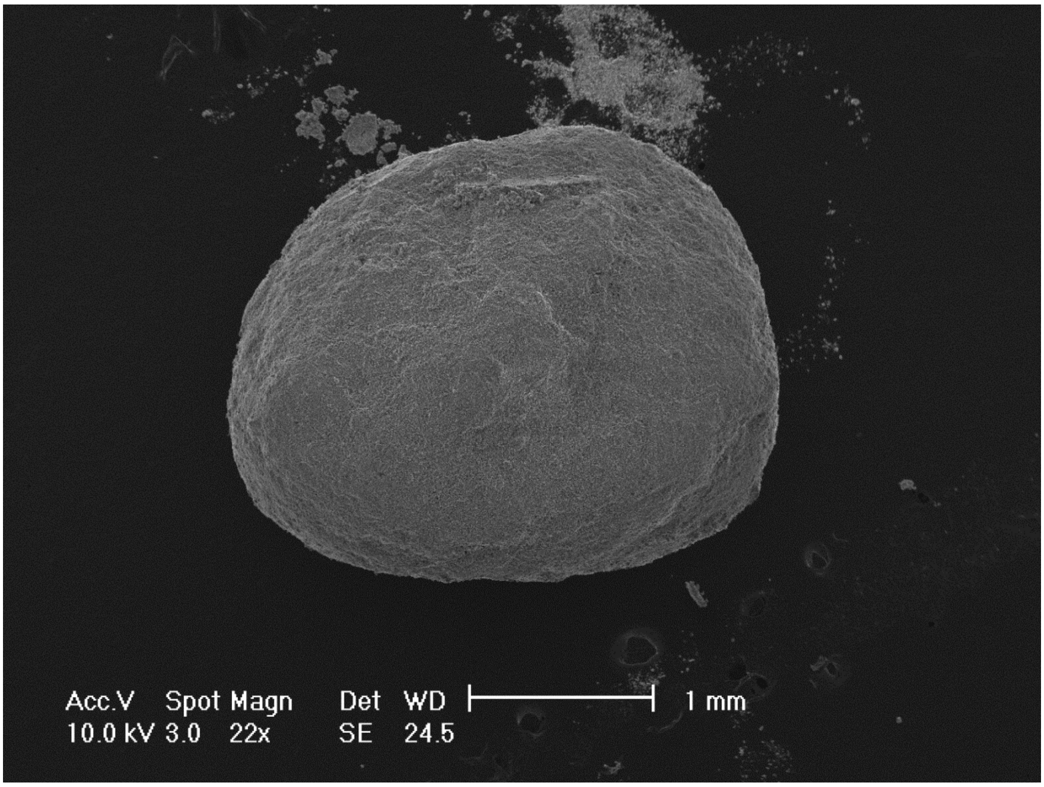

c)

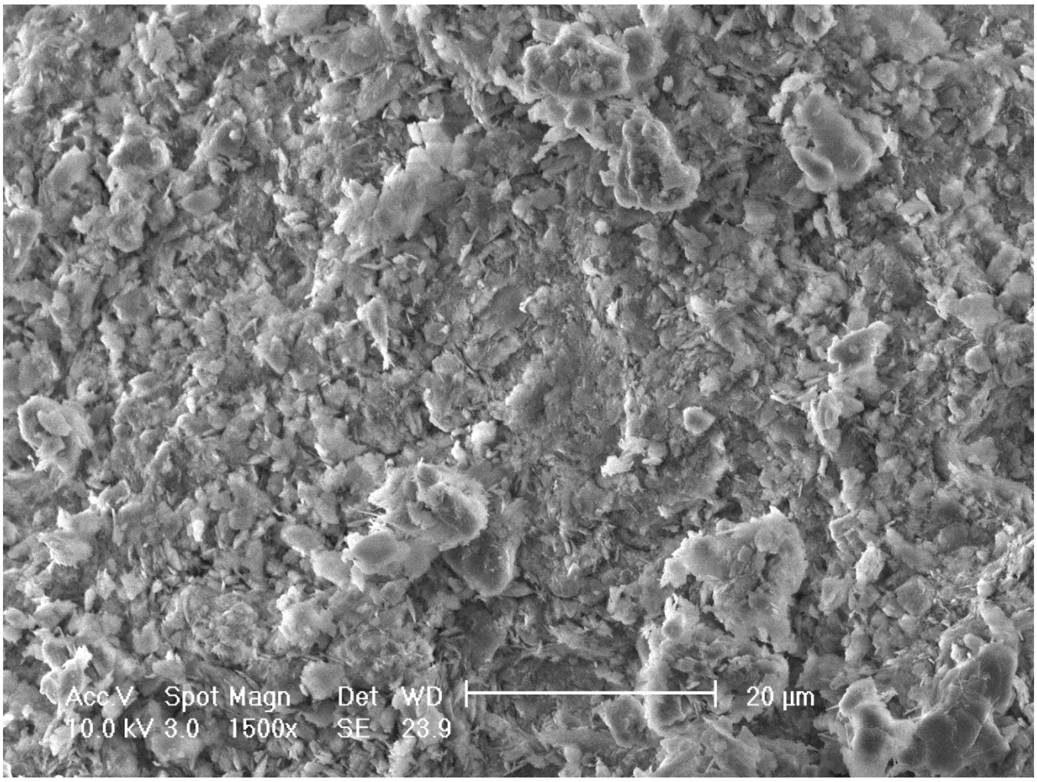

d)

Figure 4 SEM images of decomposed tuff granules surfaces from a)-b) top and c)-d) bottom of the landslide.

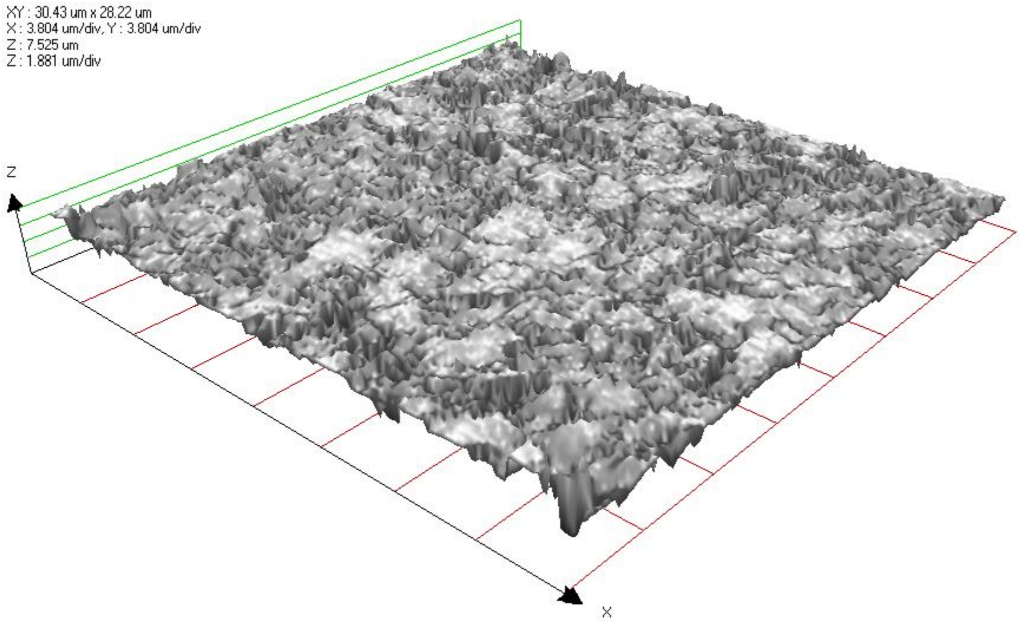

Figure 5 Typical flattened interferometer image of the surface of a granule for the calculation of the root mean square roughness.

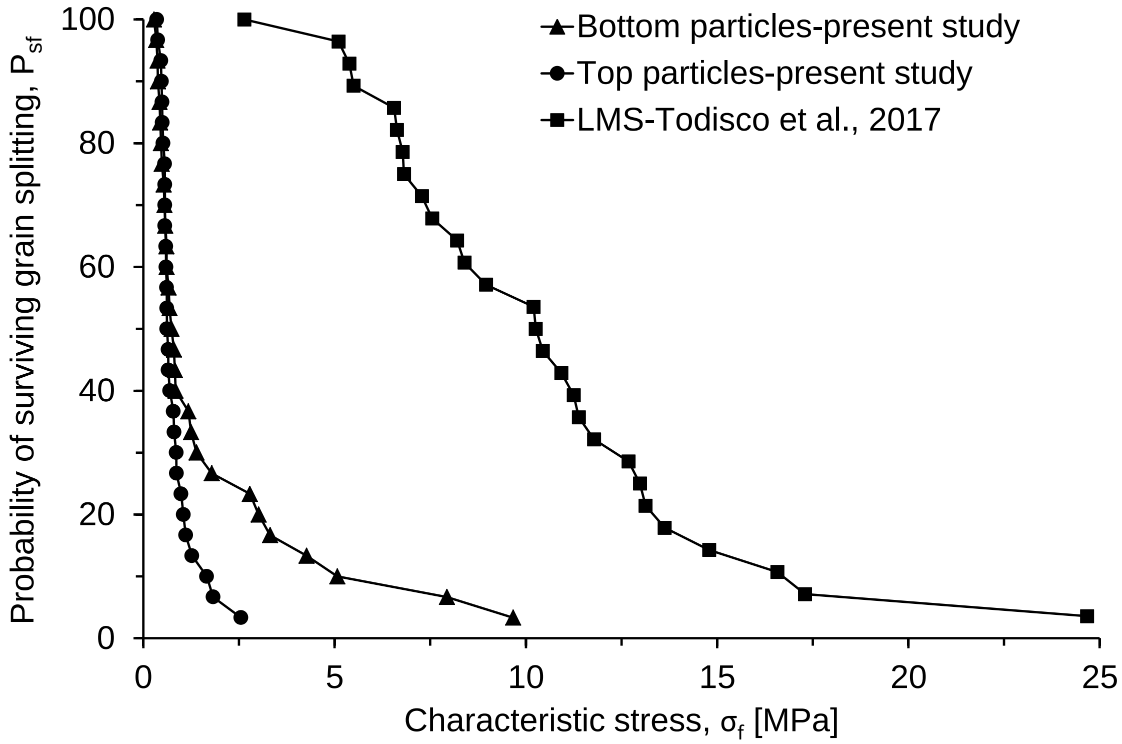

Figure 6 Single-particle crushing test results on top and bottom granules and crushed limestone (LMS) grains.

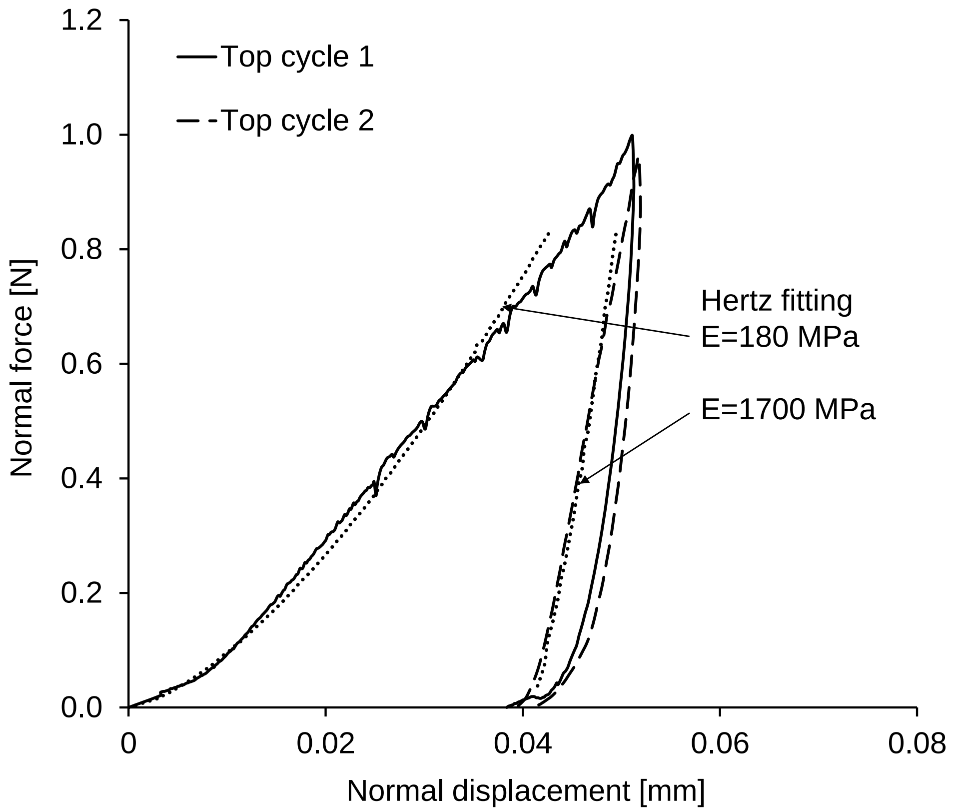

Figure 7 Normal force-displacement relationship of a pair of granules from the top of the landslide and corresponding Hertzian fitting

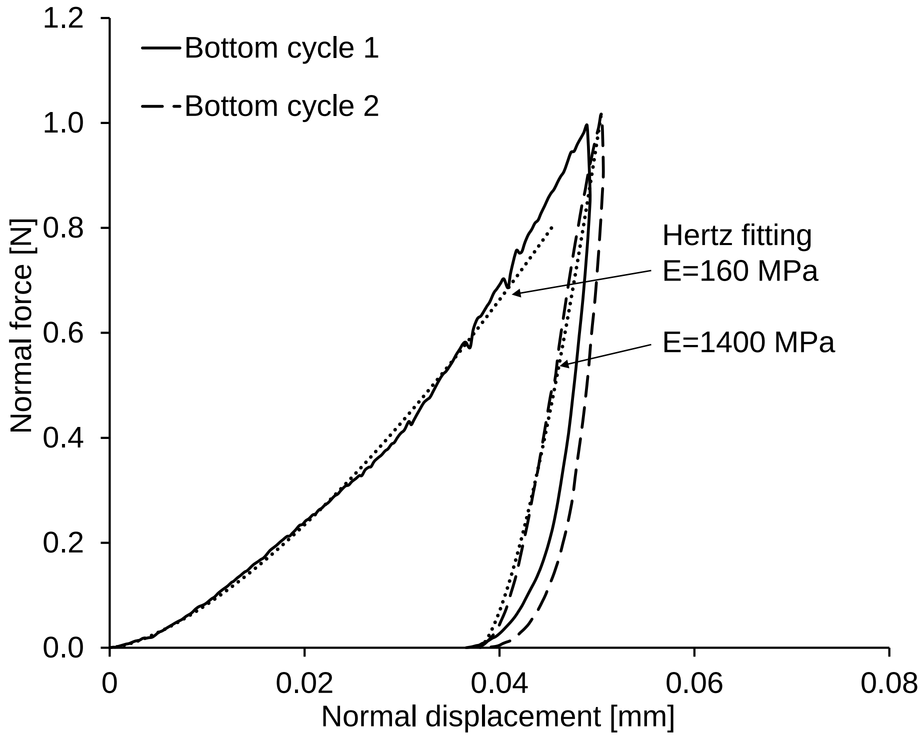

Figure 8 Normal force – displacement relationship of a pair of granules from the bottom of the landslide and corresponding Hertzian fitting

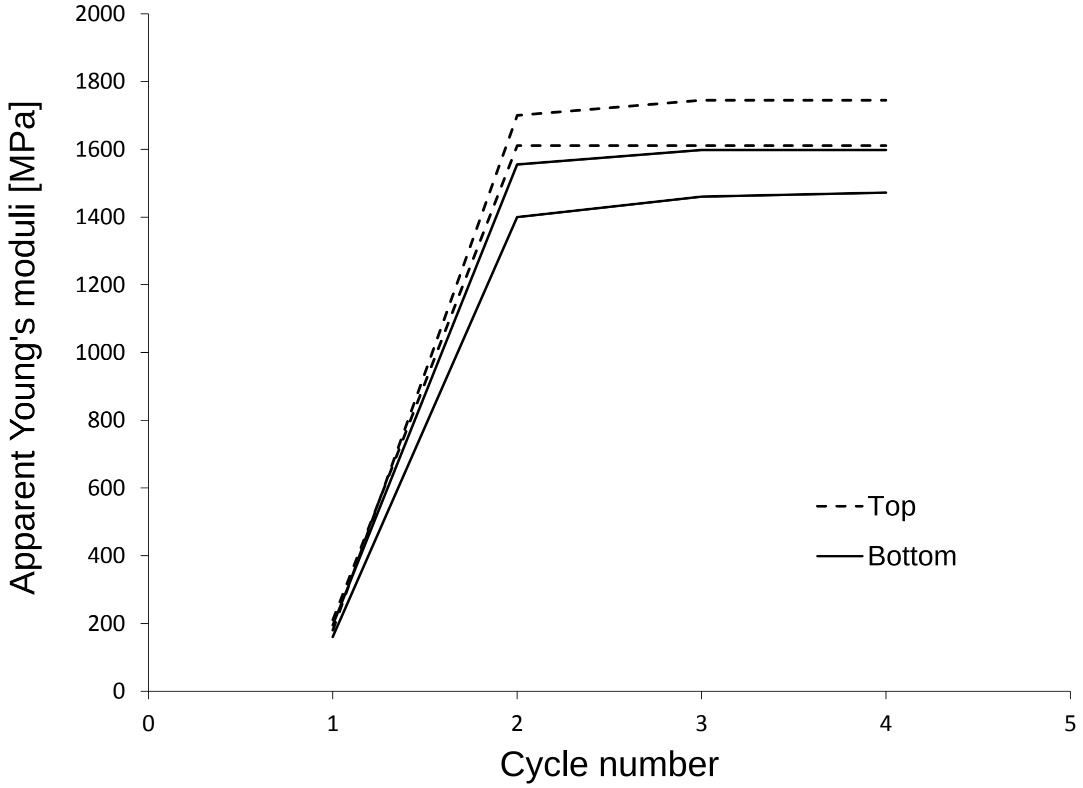

Figure 9 Effect of cycle number on the apparent Young’s moduli at the contacts of decomposed tuff granules based on normal loading tests

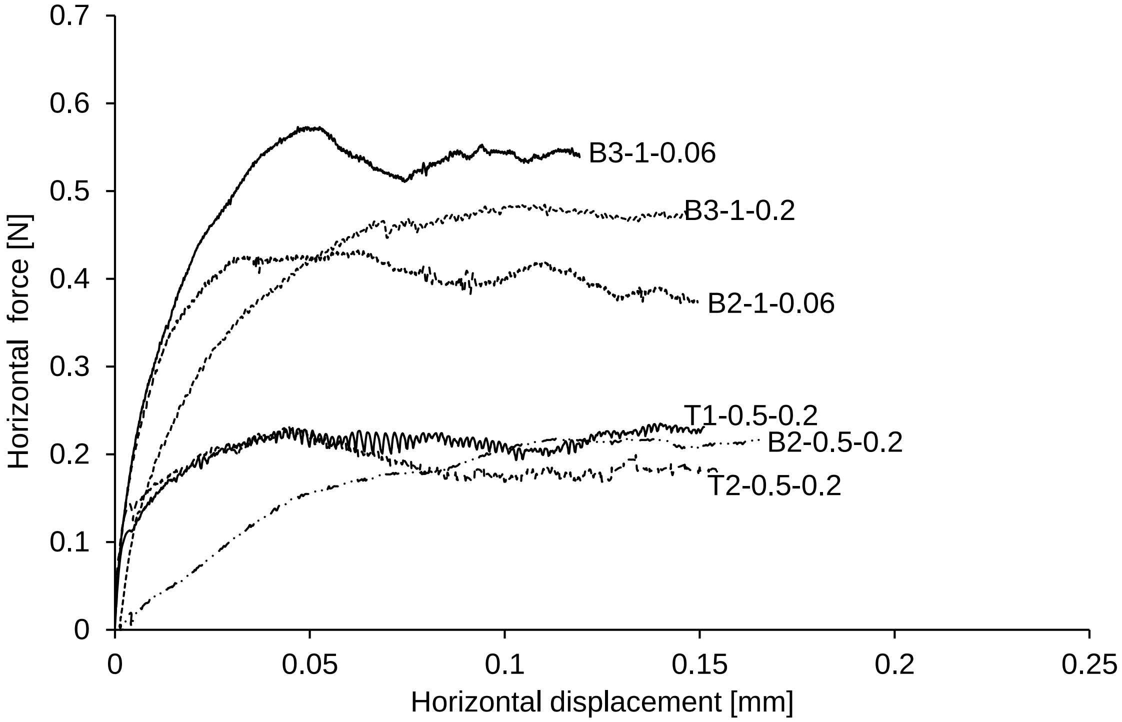

Figure 10 Typical plots of horizontal force-displacement relationship of pairs of granules from monotonic inter-particle shearing tests.

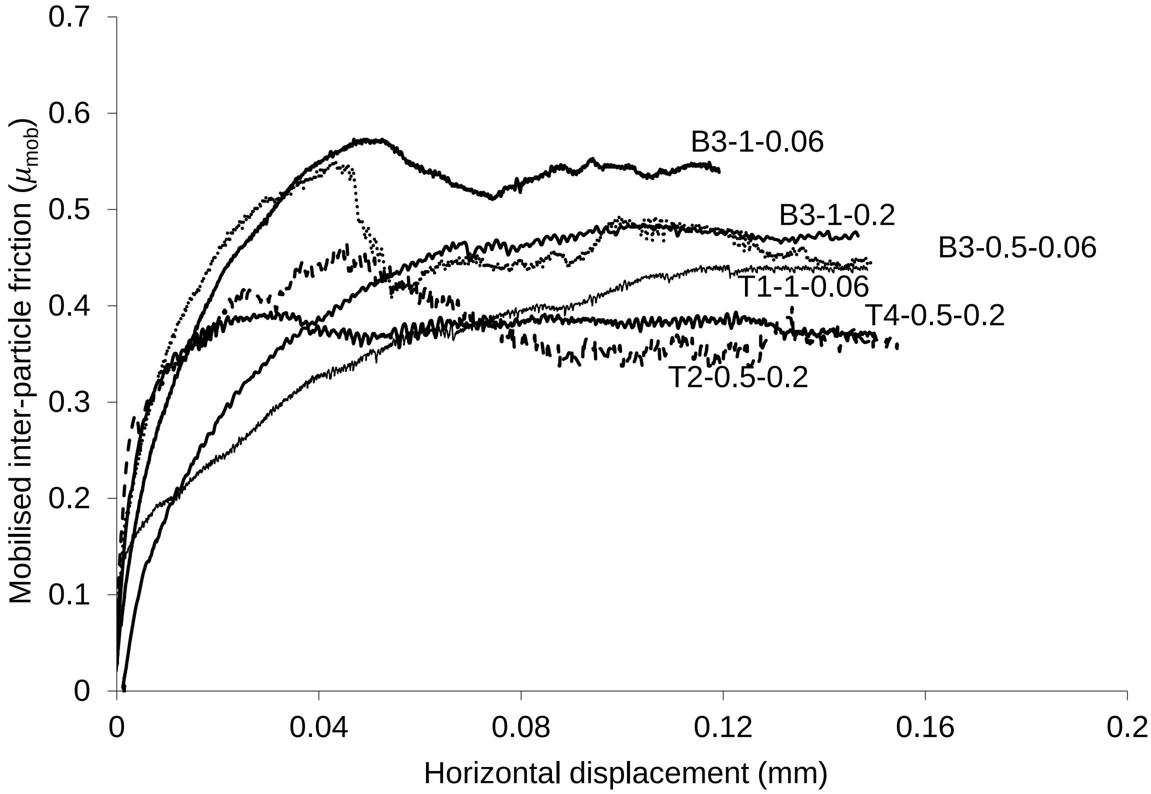

Figure 11 Typical plots of mobilised inter-particle friction angle-horizontal displacement from monotonic inter-particle shearing tests.

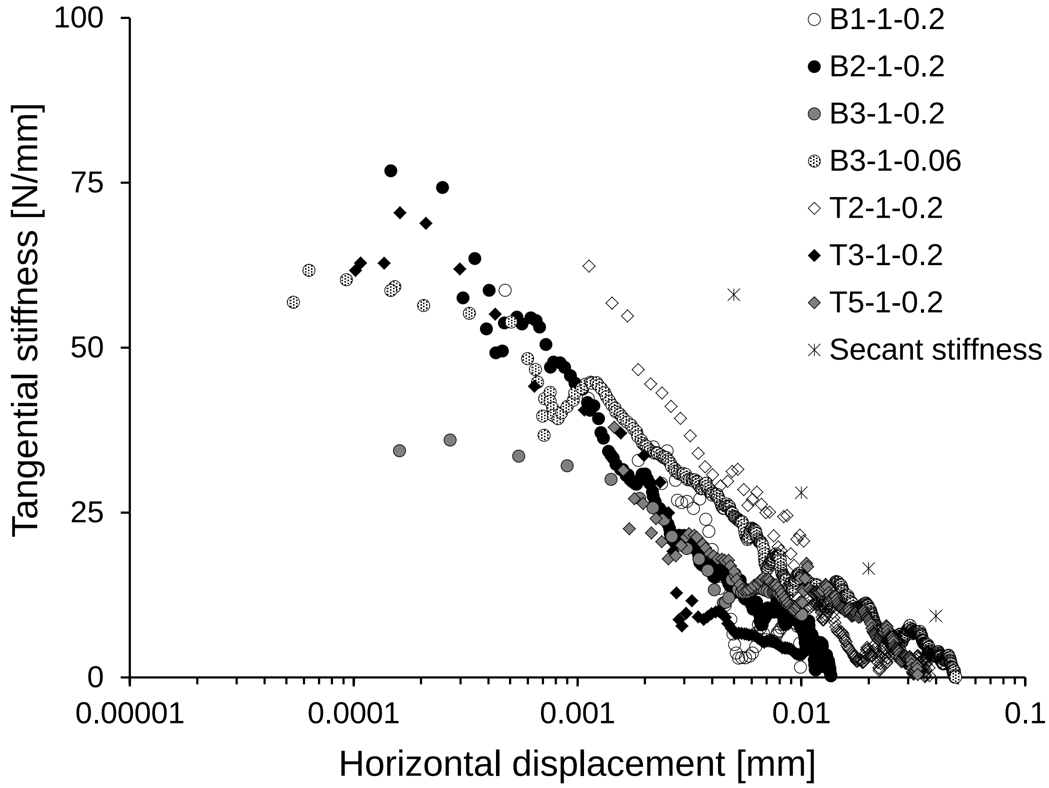

Figure 12 Typical plots of tangential stiffness against the horizontal displacement from monotonic inter-particle shearing tests (in the same figure secant stiffness values based on cyclic shearing tests are also plotted for comparison).

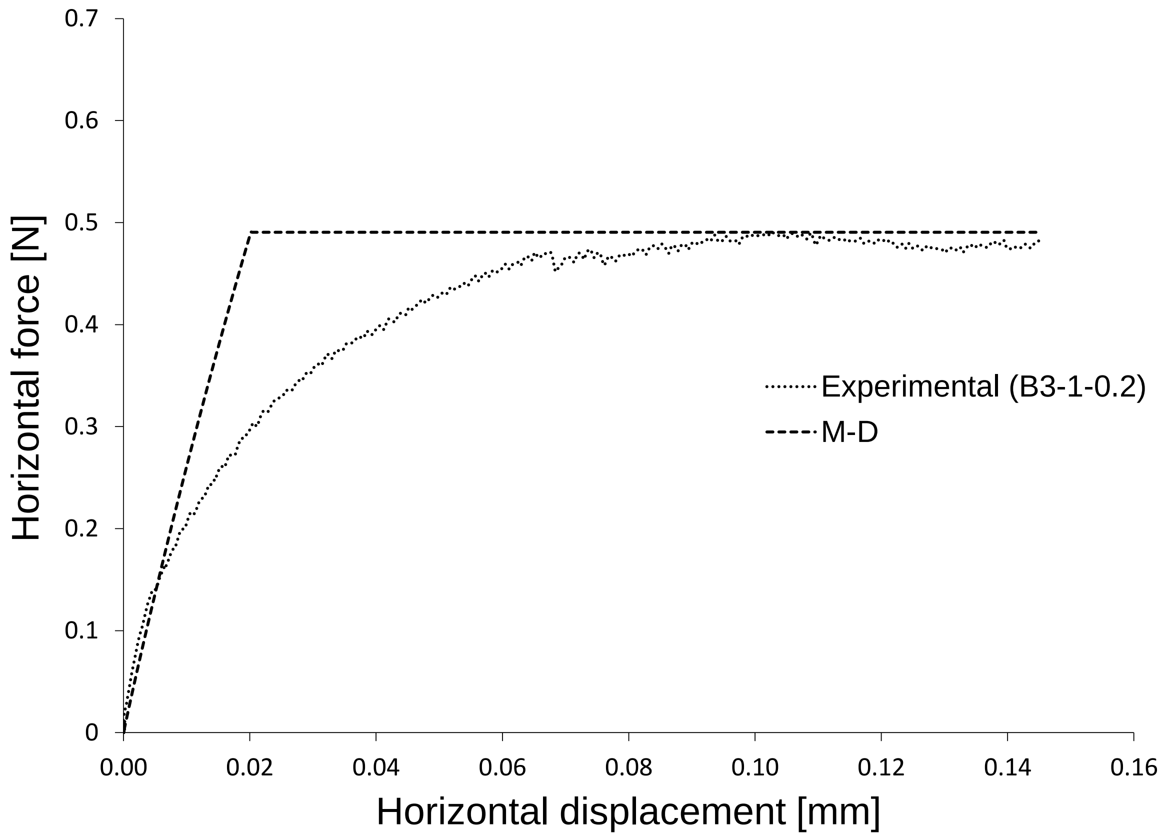

Figure 13 Comparison between an experimental horizontal force – displacement curve and the theoretical curve computed based on the Mindlin and Deresiewicz (M-D) model

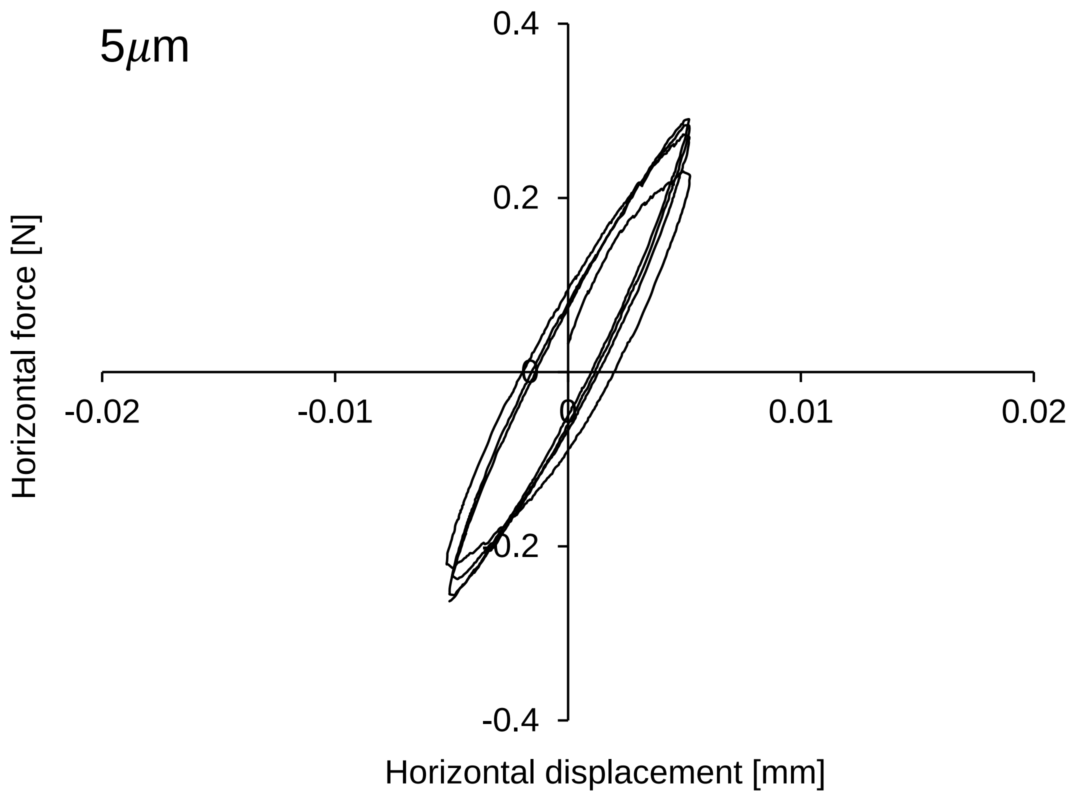
5μm
0.4
0.2
0
-0.2
-0.4
-0.02
-0.01
0
0.01
0.02
Horizontal force [N]
Horizontal displacement [mm]

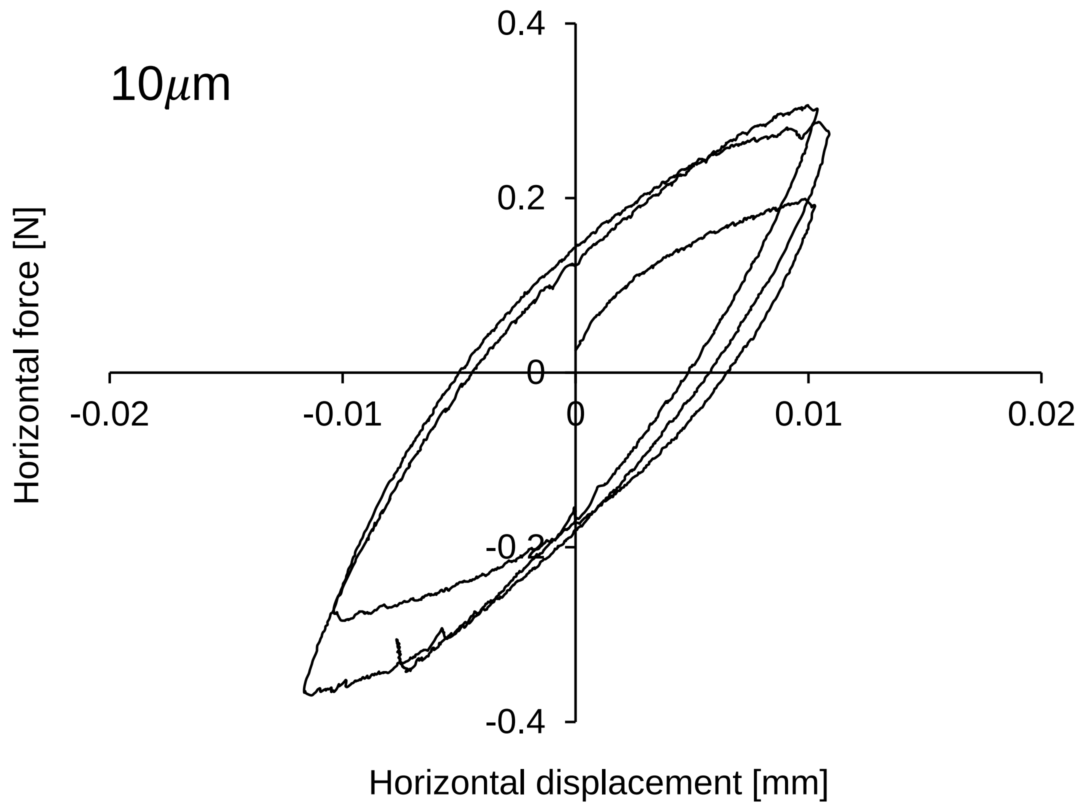
10μm
0.4
0.2
0
-0.2
-0.4
-0.02
-0.01
0
0.01
0.02
Horizontal force [N]
Horizontal displacement [mm]

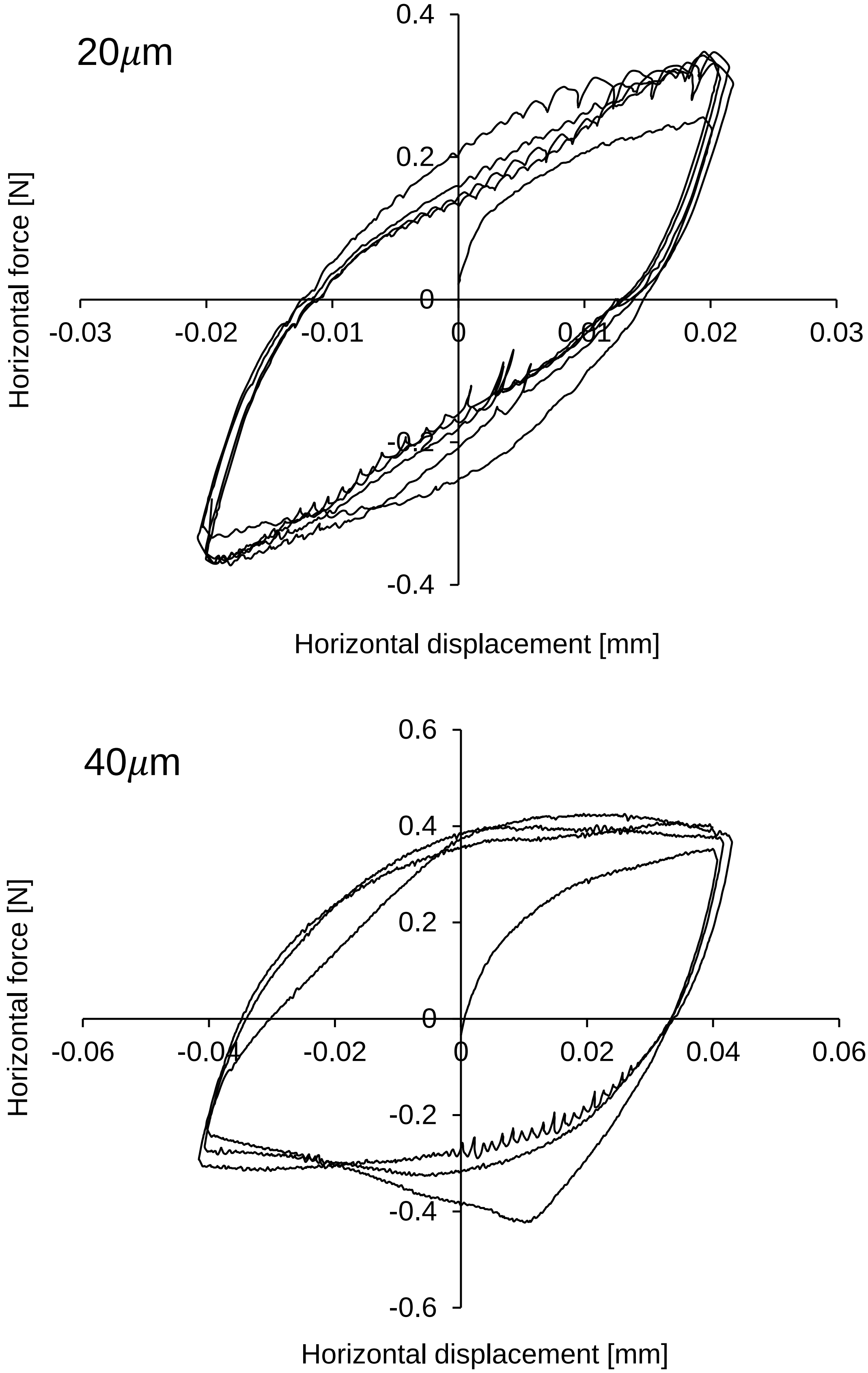

Figure 14 Cyclic inter-particle shearing tests on pairs of granules